# Compact, Low-Profile, Linearly and Circularly Polarized Filtennas Enabled with Custom-Designed Feed-Probe Structures

Ming-Chun Tang, *Senior Member, IEEE*, Dajiang Li, *Student Member, IEEE*, Yang Wang, Kun-Zhi Hu, *Student Member, IEEE*, and Richard W. Ziolkowski, *Life Fellow, IEEE*

***Abstract*— Compact, low-profile, linearly (LP) and circularly polarized (CP) patch-based filtennas are realized with a custom-designed coupling probe. It introduces a deep null at both the lower and the upper band edges of the filter response. These two nulls facilitate a quasi-elliptic bandpass behavior and can be independently controlled to achieve sharp band-edge skirts and high out-of-band suppression levels. The CP version evolves from the LP design by introducing a T-shaped near-field resonant parasitic (NFRP) element near the probe to create two transmission paths with an inherent 90° phase difference. Its presence facilitates the simultaneous excitation of the $TM_{10}$ and $TM_{01}$ modes of the patch without the need for any power divider or phase delay line, reducing the design complexity and lowering the insertion loss. Prototypes were fabricated, assembled, and tested. The measured results agree well with their simulated values. They are low profile (0.03 $\lambda_0$ height) and compact in size (0.04 $\lambda_0^2$ footprint). The LP and CP prototypes exhibit, respectively, a 10-dB fractional impedance bandwidth of 7% and an overlapping axial ratio fractional bandwidth of 4.5%. Excellent measured performance characteristics are demonstrated including flat passband realized gain values and filter responses with sharp roll-off rates and high out-of-band suppression levels.**

***Index Terms*— Circularly polarized antennas, compact antennas, filtennas, linearly polarized antennas, low-profile antennas, near-field resonant parasitic elements**

## I. Introduction

With the rapid expansion in modern wireless communication technologies, progress continues towards antenna systems that are more compact, multifunctional with high efficiencies, and more easily integrated with the electronics. The recent emergence of filtennas has resulted [1]-[28]. They represent the advantageous integration of the antenna and filter into a single compact module. They possess attractive features such as a controllable passband frequency response in both their reflection coefficient and realized gain values.

The current existing methods to accomplish filtenna designs can be generally divided into the four categories. The first approach is to organically combine the filter structures with the radiators. For instance, these filtennas can be realized by replacing the last stage of a filter network with a single radiator [1]–[9]. However, they usually require multiple resonators placed in series and, hence, they typically occupy a large area. On the other hand, they can also be realized by inserting an extra filter into the antenna as its feed network [10]-[15]. However, this style introduces additional insertion loss from its presence. The second approach is to introduce notches on the radiators such as etching slots on the radiating patches [16-18] or employing defected ground structures (DGSs) [19]. Although using DGSs avoid the insertion losses from the filter circuits, their in-band realized gain values are usually lower than those of the original antennas since the notches introduce scattering losses [19]. The third approach is to add parasitic elements to obtain the desired filter characteristics. For example, stacked parasitic patches [20]-[22] or shorting pins [20], [22] were introduced into the antennas to generate radiation nulls near the operational band to realize the filtering responses without degrading their in-band performance. However, these designs are multilayered with or without the air layers and have tall profiles. The fourth approach utilizes elaborate feeding structures, e.g., coupling probes [23], H-shaped feedlines [24], multi-stub feedlines [25], transverse stubs [26], and parasitic non-radiative strips [27], [28]. However, they take up a large transverse area and/or increase the overall complexity of the feed network. Therefore, it remains a challenge for a filtenna to realize an excellent filtering response while still maintaining a simple, compact, and low-profile configuration.

Benefitting from the development of a custom-designed coupling probe, compact, low-profile, linearly (LP) and circularly polarized (CP) patch-based filtennas are reported in this paper that operate around 2.0 GHz. This simple probe not only introduces an additional resonant mode that increases the operational impedance bandwidth, but it also creates two deep radiation nulls that improve the out-of-band rejection of its filter performance without introducing any additional loss [10-15, 19], and without increasing the antenna's profile [20-22], overall electrical size [1-9, 23-28], or design

Manuscript received on 3rd, September, 2019; revised on 20th, December, 2019, and revised on 24th, February, 2020; and accepted on 17th, March, 2020…

This work was supported in part by the National Natural Science Foundation of China contract number 61922018, in part by the Graduate Scientific Research and Innovation Foundation of Chongqing, China contract number CYB19059, in part by the Chongqing Natural Science Foundation contract number cstc2019jcyjjqX0004, and in part by the Australian Research Council grant number DP160102219.

M. -C. Tang, D. Li, Y. Wang, and K. Hu are with the Key Laboratory of Dependable Service Computing in Cyber Physical Society Ministry of Education, School of Microelectronics and Communication Engineering, Chongqing University, Chongqing 400044, China (e-mail: tangmingchun@cqu.edu.cn);

R. W. Ziolkowski is with the University of Technology Sydney, Global Big Data Technologies Centre, Ultimo NSW 2007, Australia (e-mail: richard.ziolkowski@uts.edu.au).

complexity [23-28]. These two nulls facilitate a quasi-elliptic bandpass behavior and can be independently controlled to achieve sharp band-edge skirts and high out-of-band suppression levels. The probe's unique characteristics facilitate the realization of simple LP and CP filtennas without increasing their total profile or the complexity of their feed networks while maintaining their compact physical sizes and high in-band realized gain values. The LP filtenna and its operating mechanisms are discussed first. The CP filtenna evolves next from this LP one by adding a T-shaped near-field resonant parasitic (NFRP) element to realize the requisite 90° phase difference between the resulting modal currents on the patch. The presence of the NFRP element further enhances the impedance bandwidth while maintaining a superior filter performance. Both filtennas are low profile (0.03 $\lambda_0$) and compact in size (0.04 $\lambda_0^2$) at its center frequency (wavelength $\lambda_0$) while maintaining an excellent quasi-elliptic filter response. Prototypes of the LP and CP designs were designed, fabricated, and tested. It will be demonstrated that the measured and simulated results are in good agreement.

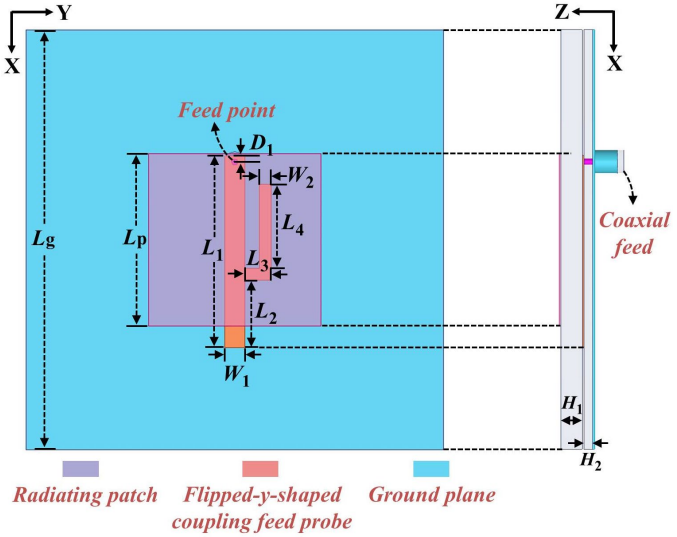


Fig. 1 LP filtenna configuration and its optimized design parameters in millimeters: $L_1$ = 31.1, $L_2$ = 11.0, $L_3$ = 4.3, $L_4$ = 13.6, $L_p$ = 28.0, $L_g$ = 68.0, $W_1$ = 3.2, $W_2$ = 1.9, $H_1$= 3.18, $H_2$ = 1.27, $R_1$ = 0.65, and $D_1$ = 1.4.

## II. LP FILTENNA

The LP filtenna configuration is illustrated in Fig. 1 along with its optimized dimensional parameters. The ground plane is square with a side length of $L_g$ = 68.0 mm. Two square dielectric blocks of the same size are centered and stacked on it. Both substrates are Taconic RF-60 TC with a relative dielectric constant $\varepsilon_r$ = 6.15, loss tangent tan $\delta$ = 0.002, and with a 0.017-mm-thick copper cladding. The lower surface of the bottom substrate resides directly on the ground plane. A square radiating patch with a side length of $L_p$ = 28.0 mm is centered on the upper surface of the top substrate with a thickness of $h_1$ = 3.18 mm. The thickness of the bottom substrate is $h_2$ = 1.27 mm; it is different from the top one to achieve better impedance matching [29]. The total height is thus 4.45 mm, which is 0.03 $\lambda_0$ at 2.0 GHz.

The coupling probe lies on top of the bottom substrate (equivalently on the bottom surface of the top substrate) directly beneath the radiating patch. Its flipped-y shape was custom-designed to improve the overall frequency selectivity. Its main strip is oriented along the *x*-axis. A 50 Ω coaxial cable with a center conductor radius $R_1$ = 0.65 mm was selected to feed the filtenna. The coax outer wall is grounded on the bottom of the ground plane; its center conductor extends vertically through the bottom substrate and is attached to the main strip. The position of the feed point, i.e., the midpoint of that conductor, is centered on the main strip of the probe along the *y*-direction and is offset from its top edge along the *x*-direction by the distance, $D_1$. The feed point and the lengths of the probe pieces are adjusted to achieve very good impedance matching.

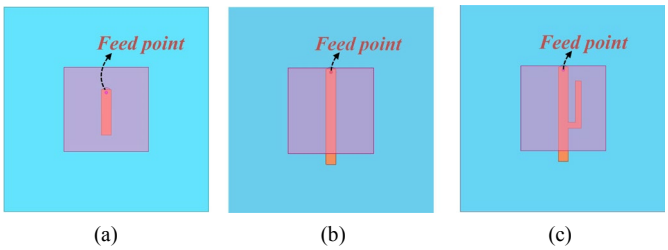


Fig. 2 Evolution of the coupling probe of the planar LP filtenna through three patch antenna iterations. (a) Ant. I, (b) Ant. II, and (c) Ant. III, the final design.

### *A. Operating Mechanisms*

The operating mechanisms of the LP filtenna and the advantages of the final coupling probe design are illustrated by comparing their evolution through three different planar designs. They are all patch antennas fed by a: (I) conventional short L-probe; (II) longer L-probe; and (III) flipped-y-shaped probe. The basic configurations of these three antennas are illustrated in sequence in Fig. 2 for ease of comparison. Fig. 3 gives the simulated reflection coefficient and realized gain values as functions of the source frequency for these three designs.

First, as shown in Fig. 2(a), Ant. I is based on a conventional short L-probe. It achieves a single resonance at 2.0 GHz with its peak realized gain being 5.9 dBi. Because its height (0.03 $\lambda_0$) is a bit more than 3 times shorter than a standard L-probe (e.g., with the center conductor length giving a 0.1 $\lambda_0$ height) [30], its fractional bandwidth (FBW), 3.5%, is about 10 times smaller [30]. Moreover, both the $|S_{11}|$ and realized gain values have only a gradual decrease when the frequencies are out of the passband. Thus, the observed filter response is poor.

Second, a longer L-probe is adopted in Ant. II, while the remaining dimensional parameters were maintained unchanged. It is clear from Fig. 3(b) that the longer probe induces a deep radiation null in the higher frequency portion of its response. It arises from the stronger coupling between the patch and the L-probe and has an associated improved selectivity from a higher suppression level outside of the upper stopband. Hence, the filter performance is much improved.

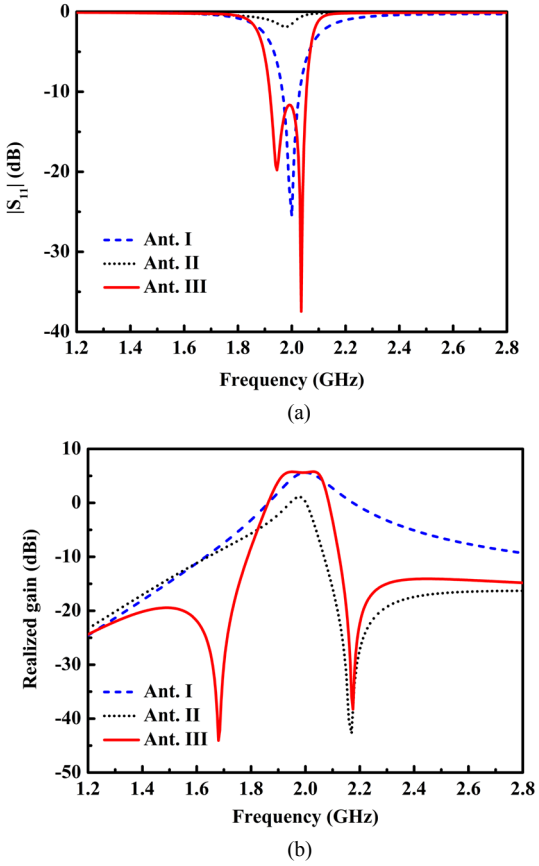


Fig. 3 Simulated results for the three patch antenna iterations as functions of the source frequency. (a) $|S_{11}|$ values. (b) Realized gain values.

To explain the appearance of this radiation null, an equivalent circuit for Ant. II is presented in Fig. 4(a). The term $R_{rad}$ is the radiation resistance of the patch, and $L_p$ and $C_p$ are its equivalent inductance and capacitance [31]. The inductance $L_n$ is produced by the L-probe itself, and the capacitance $C_n$ arises from the capacitive coupling between the probe and the patch [32]. The radiation resistance of the patch is replaced by one port to study the transmission characteristics of Ant. II. As shown in Fig 4(b), the reflection and transmission coefficients then indicate the presence of one transmission pole in the passband and one transmission zero (equal to a radiation null in antenna designs) in the upper stopband. The elements $L_p$ and $C_p$ combine to produce the transmission pole ①, and the $L_n$-$C_n$ tank sub-circuit contributes the transmission zero ②.

To verify this circuit explanation, the position of the L-probe, i.e., the distance $P_0$ between the feed-end of the L-probe's strip and the upper-edge of the patch, and the length $L_1$ of L-probe, were investigated. As shown in Fig. 5(a), when $P_0$ decreases so that these two edges are closer together with $L_1$ fixed, the filter behavior is improved, i.e., a faster roll-off rate at the upper band edge is attained. This behavior is equivalent to an increase in $C_n$ in Fig. 4(a). Similarly, as depicted in Fig. 5(b), the capacitive coupling is again enhanced when $L_1$ is increased with $P_0$ fixed. A red-shift of the null is then clearly attained. Although an enhanced selectivity at the upper band edge is obtained by choosing a proper position and a suitable length of the L-probe, the impedance matching deteriorates and the performance of the lower stopband is still unsatisfactory. Moreover, the observed operational bandwidth is substantially limited on account of only one resonance in the passband.

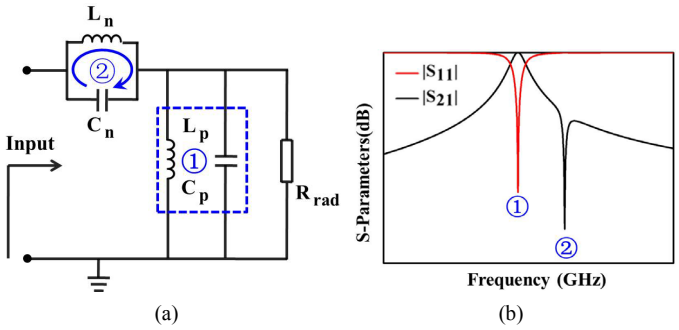


Fig. 4. The corresponding equivalent circuit (a) and its response (b) for Ant. II.

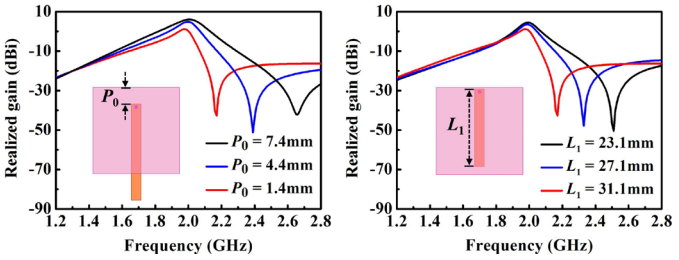


Fig. 5 Simulated realized gain values of Ant. II when two important design parameters are varied. (a) The distance $P_0$ between the feed-end of the L-probe strip and the upper-edge of the patch. (b) The length $L_1$ of the L-probe strip.

A flipped-L-shaped open-end stub is then attached to the main strip of the original L-probe as shown in Fig. 2(b) to form a flipped-y-shaped coupling probe of Ant. III. It is the final design and is illustrated in Fig. 2(c). Referring to Fig. 3(a), a new resonance mode is obtained; it is directly associated with the flipped-y-shaped probe. This resonance is located close to the original patch resonance mode, which was observed in Ant. I. These adjacent modes desirably combine to form a wider passband. Moreover, the patch has a significant loading effect on the probe [31]. The radiation of the patch dominates over the entire passband and results in good broadside radiation patterns, even at the frequency of the probe mode. Consequently, a desirably flat realized gain is obtained in the passband. Additionally, as Fig. 3(b) indicates, a new radiation null is created near the lower band edge. It arises from the well-known property that a quarter-wavelength open-end transmission line can realize a transmission zero, which is equivalent to obtaining a radiation null in an antenna design [33]. In particular, it was determined that when the total electric length $L_3$+$L_4$ is one-quarter wavelength, the lower frequency realized gain null occurs at

$$f_n = \frac{c}{4(L_3 + L_4)\sqrt{\varepsilon_{re}}} \quad (1)$$

where $c$ is the speed of light in free space, and $\varepsilon_{re}$ denotes the effective dielectric constant of the substrate. Calculating (1) with the optimized parameters given in Fig. 1, one obtains $f_n$ = 1.69 GHz, which agrees quite well with the numerically

obtained value, 1.71 GHz. Consequently, the flipped-L-shaped open-end stub is responsible for the appearance of the lower frequency null.

Finally, it was concluded that this custom-designed feed probe not only broadens the impedance bandwidth, but it also more sharply defines the realized gain passband with its introduction of a realized gain null at the lower and upper edges of its operational frequency band. This behavior is equivalent to a quasi-elliptic bandpass filtering response. Moreover, this improved filter response occurs with a peak realized gain of 5.9 dBi, essentially the same value obtained with Ant. I, the simple L-shaped probe driven patch antenna [30]. Note that while the custom-designed probe significantly improves the filter response, it does not diminish the peak realized gain value.

*B. Current Distributions and Parametric Study*

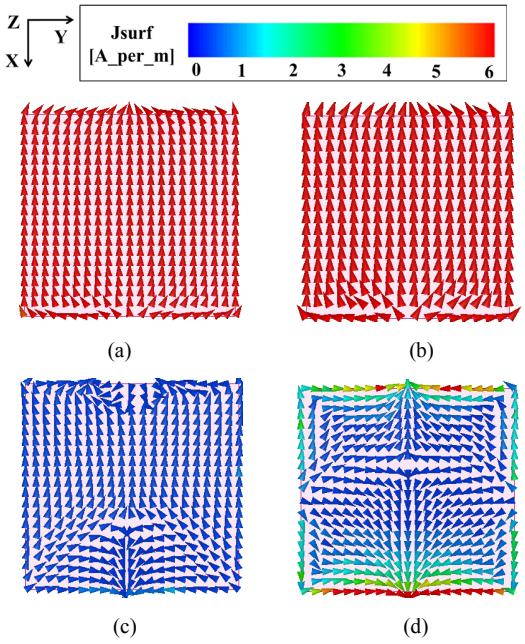


Fig. 6 The electric current distributions on the patch of the optimized LP filtenna at the resonance frequencies: (a) 1.95 and (b) 2.04 GHz, and at the frequencies of realized gain null: (c) 1.68 and (d) 2.18 GHz.

The current distributions on the patch of the optimized LP filtenna, i.e., the optimized version of Ant. III, are given in Fig. 6 at the four frequency points corresponding to the two resonances (1.95 and 2.04 GHz) in the passband and at the two nulls in the realized gain values (1.68 and 2.18 GHz). As observed in Figs. 6(a) and (b), there are strong and uniform current distributions oriented along the x-axis on the radiating patch at both resonance frequencies. They explain the flat realized gain values shown in Fig. 3(b). On the other hand, the current distributions on the patch at both radiation nulls in Figs. 6(c) and (d) are quite weak. They explain the very low realized gain levels at those null frequencies. Notice that the current distributions on the patch shown in Fig. 6(d) are almost completely out-of-phase with those associated with the upper resonance frequency. This feature further improved the upper stopband rejection of the broadside radiated power.

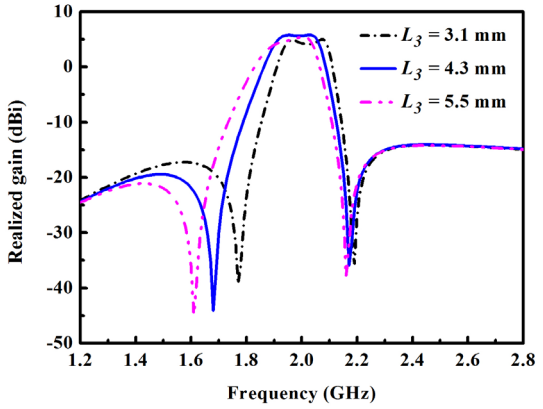


(a)

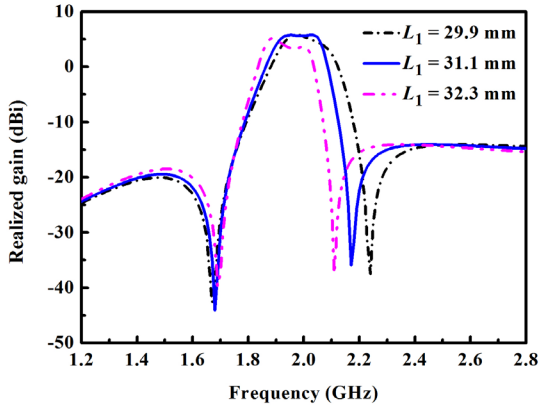


(b)

Fig. 7 Simulated realized gains values of the LP filtenna design as functions of the source frequency when the design lengths (a) $L_3$ and (b) $L_1$ of the flipped-y-shaped probe are varied.

Parametric studies were carried out to further analyze the key design parameters' effects on the two realized gain nulls. Fig. 7 shows that the simulated realized gains as functions of the source frequency when the length $L_3$ of flipped-L-shaped open-end stub and the length $L_1$ of the main strip of the feed probe are varied. When $L_3$ increases from 3.1 to 5.5 mm, the lower null in Fig. 7(a) clearly exhibits a red-shift, while the upper one remains almost unchanged. Similarly, when $L_1$ increases from 29.9 to 32.3 mm, the upper null in Fig. 7(b) also exhibits a red-shift, while the lower one remains almost unchanged. Therefore, the lower and upper realized gain nulls can be independently controlled by changing the parameters $L_3$ and $L_1$. This design feature of the optimized LP filtenna is advantageous since it facilitates being able to tailor the filter response for different applications.

*C. Simulated and Measured Results*

The optimized LP filtenna shown in Fig. 1 was fabricated, assembled, and measured. This prototype is shown in Fig. 8. Four polyamide pillars were utilized to fix the two substrates together, as indicated in Fig. 8(b), to ensure the mechanical stability of the filtenna during the measurement process. The impedance measurements were carried out by using an Agilent Technologies E5071C network analyzer. The far-field characteristics of the prototype, including its realized gain values and corresponding radiation patterns, were obtained

with a multi-probe spherical near field test anechoic chamber, as shown in Fig. 8(c).

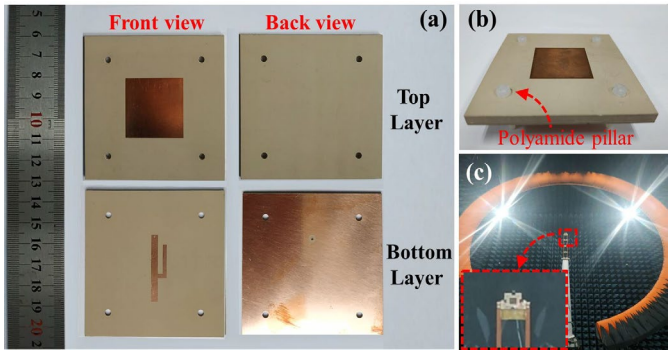


Fig. 8 Fabricated LP filtenna. (a) Front and back views of each layer before assembly. (b) 3-D isometric view after assembly. (c) Antenna under test (AUT) in the anechoic chamber.

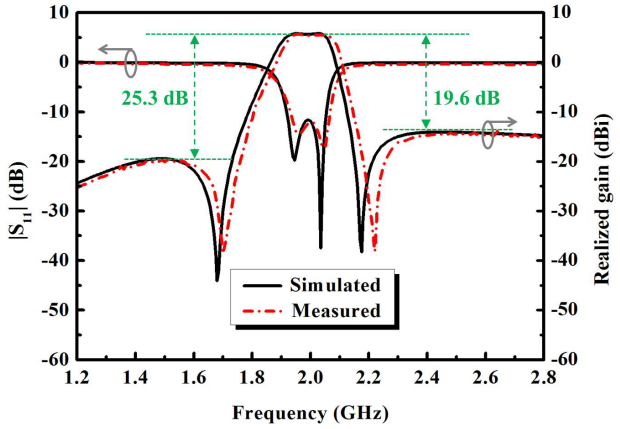


Fig. 9 Simulated and measured $|S_{11}|$ and realized gain values of the optimized LP filtenna as functions of the source frequency.

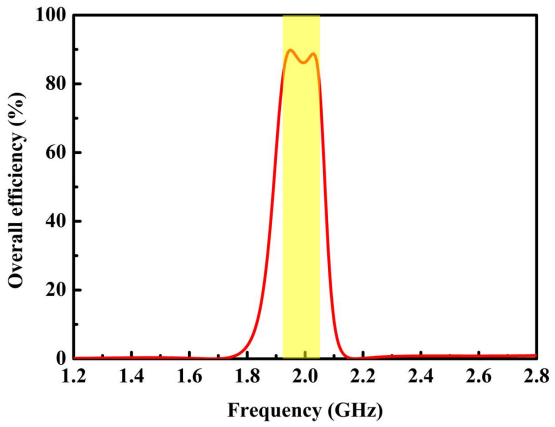


Fig. 10 The simulated overall efficiency values of the LP filtenna as a function of the excitation frequency. Its operational band is highlighted in yellow.

Fig. 9 provides the simulated and measured $|S_{11}|$ and realized gain values of the LP filtenna as functions of the source frequency. It demonstrates that the measured -10-dB FBW is 7% (1.93-2.07 GHz) in comparison to its simulated value, 6.5% (1.92-2.05 GHz). With reference to the realized gain curve, a quasi-elliptic band-pass response was obtained as predicted. The measured peak realized gain was 5.8 dBi and its average value was 5.6 dBi. Again, the measured results agree well with their simulated values. High selectivity is clearly obtained with the two deep nulls in the realized gain values located at 1.7 and 2.22 GHz. The measured out-of-band suppression levels are 25.3 dB and 19.6 dB, respectively, at the lower and upper edges of the stopband. Moreover, as is shown in Fig. 10, the simulated overall efficiency is greater than 80% across the entire operational band, 1.92−2.05 GHz.

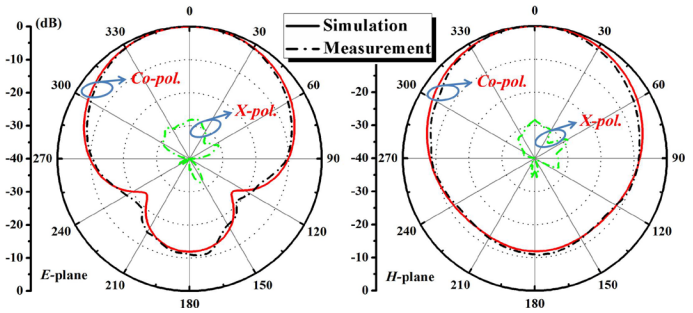


Fig. 11 The simulated and measured 2-D normalized realized gain patterns of the LP filtenna operating at 2 GHz. (a) E-plane. (b) H-plane.

Finally, Fig. 11 illustrates the simulated and measured normalized realized gain patterns of the LP filtenna. The measured results agree very well with their simulated values. It is clear that the peak realized gain is strictly along the broadside direction and the measured co-polarized fields are at least 28 dB stronger than their cross-polarized counterparts in both principal planes. Furthermore, it is noted that the measured front-to-back ratio (FTBR) value is ~11 dB, which is essentially the same as that of a standard direct-fed patch antenna of the same size.

## III. CP FILTENNA

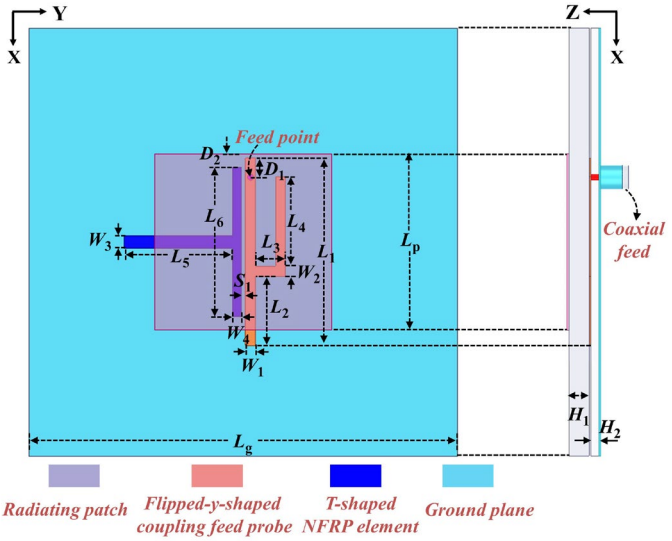


Fig. 12 CP filtenna configuration and its optimized design parameters in millimeters: $L_1$ = 29.7, $L_2$ = 10.9, $L_3$ = 4.7, $L_4$ = 14.2, $L_5$ = 17.2, $L_6$ = 23.8, $L_p$ = 28.0, $L_g$ = 68.0, $W_1$ = 1.6, $W_2$ = 1.5, $W_3$ = 2.0, $W_4$ = 1.4, $D_1$ = 3.0, $D_2$ = 2.1, $H_1$= 3.18, $H_2$ = 1.27, $R_1$ = 0.65.

Fig. 12 shows the CP filtenna configuration. It is a clear evolution from the realized LP filtenna design in Fig. 1. An

additional T-shaped NFRP element is simply printed aside the flipped-y-shaped coupling probe, while the other components remain unchanged. The T-shaped NFRP element consists of two connected straight strips that are oriented orthogonal to each other. The strip along the x-axis has the total length $L_6$ and is oriented parallel to the main strip of the feed probe. It adjusts the coupling strength between the NFRP element and the probe. The orthogonal strip is centered on that strip and has the total length $L_5$ along the y-axis. It facilitates the excitation of a fundamental resonance mode whose currents are oriented along the y-axis. The distance between the probe and NFRP element is $S_1$. Its variation helps further optimize the mutual coupling between the NFRP element and the probe to achieve good impedance matching. Additionally, because most of the NFRP element is located underneath the patch, its presence does not substantially increase the filtenna's overall transverse size. The optimized design parameters are also given in the caption of Fig. 12.

### *A. Simulated and Measured Results*

The optimized CP filtenna shown in Fig. 12 was fabricated, assembled, and measured. The fabricated prototype is shown in Fig. 13. The test equipment and test environment are the same to those shown in Fig. 8 and used to test the LP filtenna.

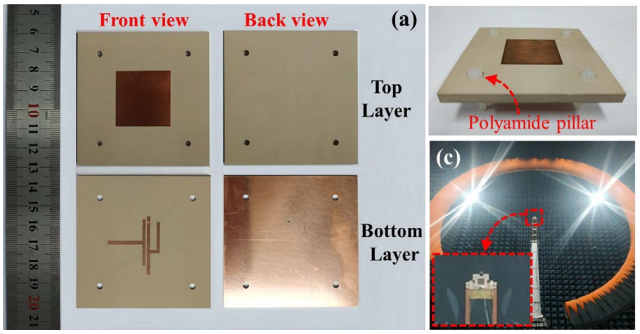


Fig. 13 Fabricated CP filtenna prototypes. (a) Front and back views of each layer before assembly. (b) 3-D isometric view after assembly. (c) AUT in the anechoic chamber.

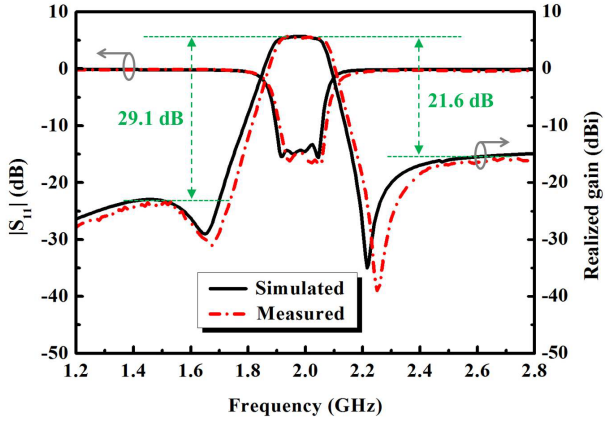


Fig. 14 Simulated and measured $|S_{11}|$ and realized gain values of the optimized CP filtenna as functions of the source frequency.

As shown in Fig. 14, the measured -10-dB FBW is 8.1% (1.9-2.06 GHz) and its simulated value is 8.0% (1.91-2.07 GHz). The measured peak realized gain value reaches 5.8 dBi and the average realized gain value is 5.6 dBi. Again, these are also consistent with their simulated ones. As with the LP prototype, high frequency selectivity is achieved in the CP filtenna due to the presence of the two nulls in its realized gain profile. They are located at 1.67 and 2.25 GHz, respectively. The measured out-of-band suppression levels are 29.1 dB and 21.6 dB, respectively, at the lower and upper edges of the passband. As is shown in Fig. 15, the simulated overall efficiency is greater than 75% across the entire operational band, 1.9−2.06 GHz.

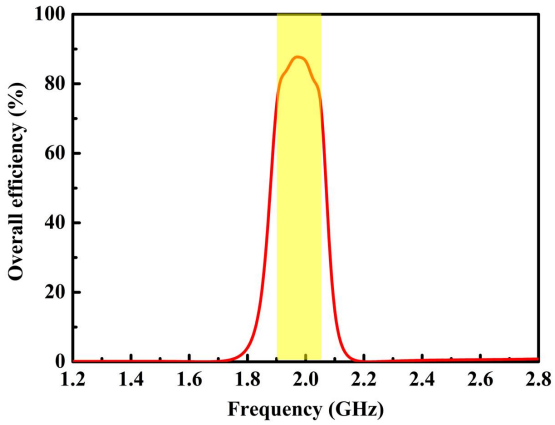


Fig. 15 The simulated overall efficiency values of the CP filtenna as a function of the excitation frequency. Its operational band is highlighted in yellow.

Fig. 16 shows the measured and simulated axial ratio (AR) values in the broadside direction as functions of the source frequency. The measured and simulated 3-dB AR bandwidths are 4.5% (1.94–2.03 GHz) and 4.0% (1.94–2.02 GHz), respectively. Thus, the measured overlapping FBW (where $|S_{11}| \leq -10$ dB and AR $\leq 3$ dB) is 4.5% (1.94–2.03 GHz). In comparison, the simulated overlapping bandwidth is 4.0% (1.94–2.02 GHz). Thus, the measured fractional bandwidth differs from the simulated one by only 0.5%. In addition, we note that the measured impedance bandwidth is wider than the AR bandwidth. The overlapping bandwidth ratio: 4.5% / 8.1% ~ 55.5%. Because this ratio is somewhat low, we considered re-optimizing the design parameters to improve it. An overlapping bandwidth ratio was attained that is 3.6% / 5.6% ~ 64%, i.e., an 8.5% improvement. However, the cost is a reduction of the overlapping bandwidth, down to 3.6%, i.e., a 20% decrease. Even so, it is still wider than that of the standard L-probe LP patch antenna shown in Fig. 1(a), 3.5%. Nevertheless, in order to emphasize that the custom-designed coupling probe is a very effective means to enhance the operational bandwidth, the filtenna design with the wider bandwidth was thus selected for experimental validation.

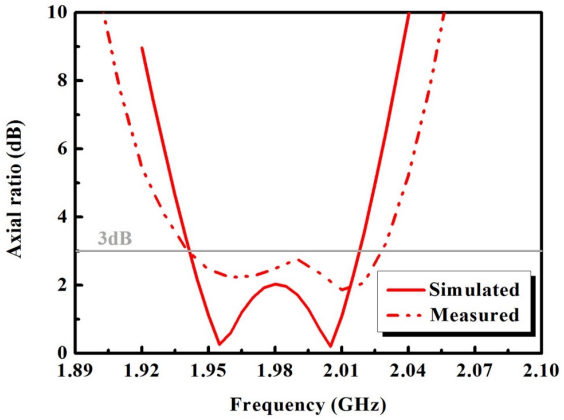


Fig. 16 Simulated and measured AR values of the CP filtenna as functions of the source frequency.

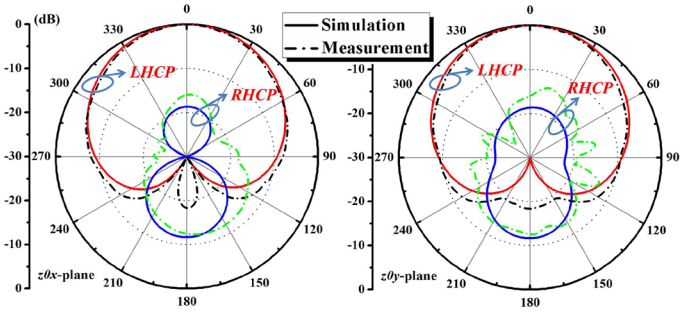


Fig. 17 The simulated and measured normalized realized gain patterns of the prototype CP filtenna operating at 2.0 GHz in the middle of its passband.

Fig. 17 illustrates the simulated and measured normalized realized gain patterns of the CP filtenna prototype. It is again clear that its peak realized gain is strictly along the broadside direction. Moreover, the measured left-handed (LH) - polarized fields are at least 16.0 dB stronger than its right-hand (RH) - polarized counterparts in the two principal planes. Furthermore, it is noted that the measured FTBR value is ~12 dB, which demonstrates that the presence of the T-shaped NFRP element has little effect on the backward radiation. The measurement results are thus demonstrated to in very reasonable agreement with their simulated values.

*B. Operating Mechanisms*

The T-shaped NFRP element operates as a current orientation-transforming resonator. It empowers the CP functionality while maintaining the filter performance. To illustrate the CP operating mechanism, the topology of the coupled probe and NFRP element is displayed in Fig. 18. One observes that there are two coupling paths from the input port to the patch. These two paths excite the two orthogonal modes, $TM_{10}$ and $TM_{01}$, of the patch. The electromagnetic energy introduced from the input port is directly coupled to the patch through the flipped-y-shaped probe as denoted by Path 1. This coupling excites the $TM_{10}$ mode of the patch with the phase $\varphi_1$. The electromagnetic energy from the input port is also coupled to the NFRP element through the feed probe with the phase $\varphi_2$, as denoted along the Path 2. This coupling then excites the orthogonal $TM_{01}$ mode of the patch with the phase delay $\varphi_3$. Known theory [34, 35] then tells us that an equal coupling level in these two paths and a 90° difference between $\varphi_1$ and the sum: $\varphi_2+\varphi_3$, enables the CP radiation mechanism. Note that this method achieves the phase along Path 2 to lag that of Path 1 by 90° without adding any extra phase delay line. Consequently, this design significantly reduces the complexity of the system and lowers the insertion loss.

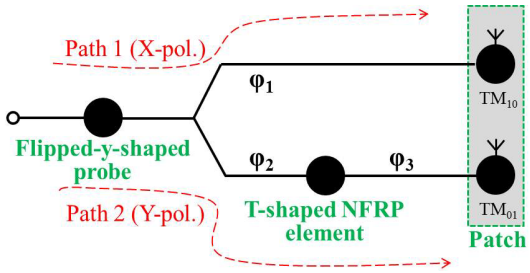


Fig. 18 Topology of the CP generation mechanism of the filtenna in Fig. 13.

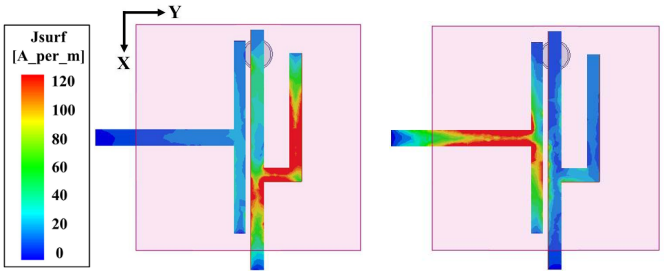


(a) (b)

Fig. 19 Simulated current distributions on the overall feed structure: feed probe and T-shaped NFRP element of the CP filtenna at its center frequency, 2 GHz, when (a) $t = 0°$, (b) $t = 90°$.

Fig. 19 shows the simulated current distributions on the NFRP element and on the feed probe of the CP filtenna at two different time (phase) values during one period of the excitation frequency. When $t$ = 0°, most of the current is concentrated on the flipped-y-shaped probe surface, primarily on its x-axis oriented pieces. Very little current is on the T-shaped NFRP element. On the other hand, when $t$ = 90°, there are very strong surface currents primarily along the y-axis piece of the T-shaped NFRP element in the –y direction. Since these two current distributions are orthogonal, the NFRP element acts as resonator that transforms the orientation of the primary current during each quarter period of the excitation frequency to its orthogonal state. Moreover, the orientations of the current distributions in Fig. 19 demonstrate that the current transformation to the -y-direction state lags 90° behind its positive x-directed state. Thus, as observed in Fig. 17, the CP co-polarization state of the filtenna is left-handed.

As with the LP design, the nulls in the realized gain values of the CP design can be separately controlled by adjusting the two structural parameters, the lengths $L_3$ and $L_1$ of the feed probe. The effects on the impedance and gain bandwidths when these lengths are varied were studied. The resulting simulated $|S_{11}|$ and realized gain values are illustrated in Fig. 20. In Fig. 20(a), the lower null exhibits a red-shift, while the upper null remains unchanged when $L_3$ is increased from 3.4 to 5.9 mm. Similarly, the upper null in Fig. 20(b) exhibits a red-shift, while the lower null remains almost unchanged

when $L_1$ increases from 28.5 to 30.9 mm. These outcomes demonstrate that the impedance and gain bandwidths are not independently controlled in this design. On the other hand, similar parametric studies of the lengths $L_5$ and $L_6$ of the T-shaped NFRP element have demonstrated that they have almost no impact on the filter performance.

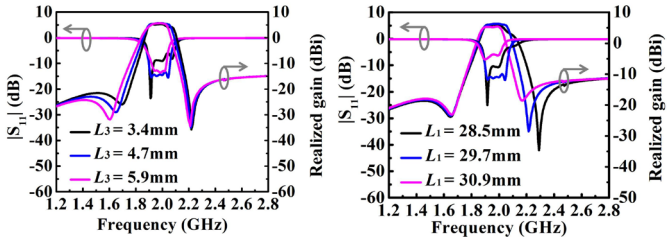


Fig. 20 Simulated $|S_{11}|$ and realized gain values of the CP filtenna design as functions of the source frequency when the design lengths (a) $L_3$ and (b) $L_1$ of the flipped-y-shaped probe are varied

## IV. Comparisons

Detailed comparisons of the performance characteristics of our LP and CP filtenna prototypes with other recently reported patch-based filtennas are given in Table I. The frequency selectivity at the lower and upper edges ($F_L$ and $F_U$) of the operating band is defined as [22]:

$$F_L = \frac{f_{10L} - f_{\Delta 30L}}{f_{10U} - f_{10L}} \qquad F_U = \frac{f_{\Delta 30U} - f_{10U}}{f_{10U} - f_{10L}} \tag{2}$$

The terms $f_{10L}$ and $f_{10U}$ are, respectively, the frequencies at which $|S_{11}|$ = -10 dB at the lower and upper edges of the passband. The terms $f_{\Delta 30L}$ and $f_{\Delta 30U}$ are, respectively, the lower and upper frequencies corresponding to the 30 dB gain suppression values with respect to the gain at the center frequency $f_0$. Better frequency selectivity is represented by smaller $F_L$ or $F_U$ values [22]. The $F_L$ and $F_U$ values for the reported LP and CP filtennas results shown in Figs. 9 and 14 are 1.73 and 1.36, and 1.5 and1.44, respectively.

We note that the radiation patches in [6]-[9] acts as the last-stage resonator of their feed networks to establish their bandpass filter performance. Because their networks are multiple resonators placed in series, these filtennas are complicated and occupy much larger spaces than our designs. The bandpass filter served as the feed network in [10], but the height of the antenna system (0.095 $\lambda_0$) is much larger than our designs. Resorting to etching two pairs of straight slots on the patch as in [16] not only requires twice the transverse size of our designs, but it also does not to extend to a CP filtenna design. The hybrid methods in [20], [22], [24], employ either stacked patches, shorting pins, or H-shaped feedlines that are tailored to introduce nulls in the realized gain profiles near the filter's passband edges. A vertical F-shaped coupling probe is adopted in [23] to obtain the filter response. Even though these systems realized the bandpass filter while maintaining the in-band radiation performance, they are multi-layered and even include air gaps [20, 22-24], which make their configurations complicated and high-profile. In contrast to the above patch-based filtennas, the developed prototypes are simple, have the smallest transverse size (0.04 $\lambda_0^2$) and match the lowest reported profile (0.03 $\lambda_0$). Nevertheless, they maintain excellent quasi-elliptic filter responses. Furthermore, while the efficiency values of the reported antennas in this work (80%) are not as high as those in [23] (95%), the transverse sizes and profiles of the former are much smaller than those of the latter.

Table I
Comparisons of the Performance Characteristics of the LP and CP Filtenna Prototypes with Related Patch-based Filtennas Reported in the Literature

| Refs. | Filtering methods | Pol. | Profile (*$\lambda_0$) | Transverse size (*$\lambda_0^2$) | Impedance FBW (%) | Overlapping AR FBW (%) | Average Realized Gain (dBi) | Number real. gain nulls |
|---|---|---|---|---|---|---|---|---|
| [6] | Multiple resonators cascade | LP | 0.05 | 0.65*0.62 | 14.7 | | 5.2 | 2 |
| [7] | Multiple resonators cascade | CP | 0.07 | 0.53*0.53 | 14 | 12.2 | 5.2 | 0 |
| [8] | Multiple resonators cascade | CP | 0.04 | 0.44*0.44 | 4.5 | 2.4 | 3.5 | 0 |
| [9] | Multiple resonators cascade | CP | 0.03 | 0.51*0.46 | 10.3 | 8.8 | 5.8 | 0 |
| [10] | Bandpass filter as feed network | CP | 0.095 | 0.50*0.50 | 4.5 | 4.5 | 6.1 | 1 |
| [16] | Two pairs of slots etched on the patch | LP | 0.03 | 0.35*0.24 | 7 | | 6.6 | 2 |
| [20] | Stacking patches & U-slot & shorting pin | LP | 0.11 | 0.45*0.45 | 19.6 | | 9.7 | 3 |
| [22] | Stacking patches & one pair of slots | LP | 0.13 | 1.00*1.00 | 8.7 | | 7.2 | 2 |
| [23] | Vertical F-shaped coupling probe | LP | 0.1 | 0.33*0.42 | 21.3 | | 8.2 | 2 |
| [24] | Stacking patches & H-shaped feedline | LP | 0.09 | 0.37*0.37 | 15.5 | | 9.4 | 2 |
| This work | One compact, simple feed probe | LP | 0.03 | 0.21*0.19 | 7 | | 5.6 | 2 |
| | | CP | 0.03 | 0.20*0.22 | 8.1 | 4.5 | 5.6 | 2 |

## V. Conclusion

Compact, low-profile, linearly (LP) and circularly polarized (CP) patch-based filtennas with notable performance characteristics were developed in this paper. A custom-designed coupling probe enabled the LP system. By augmenting it with a T-shaped NFRP element, the CP version was obtained in a simple fashion. It was demonstrated that the custom-designed probe facilitates the introduction of an additional resonance along with the patch resonance mode. The presence of these two resonances increased the impedance bandwidth. The probe also facilitated the realization of a null in the realized gain profile near both the lower and upper frequency edges of the passband. High frequency selectivity was thus attained with the resulting sharp band-edge skirts while maintaining a compact size ($0.21\ \lambda_0 \times 0.22\ \lambda_0$) and low profile ($0.03\ \lambda_0$). Prototypes of both the LP and CP filtennas were designed, fabricated, and measured. The measured results agree well with their simulated values. Wide impedance bandwidths, flat passband realized gain responses, excellent filter roll-off rates, and high out-of-band rejection levels were demonstrated. The LP and CP designs exhibit a measured FBW of 7% and an overlapping FBW of 4.5%, respectively. These filtennas would be useful for many space-limited wireless platforms, such as satellite communication, electronic countermeasure, and radar detection systems, since one could take advantage of their good in-band radiation and out-of-band filtering performance features to achieve compact, low-profile configurations.

## References


[1] C.-K. Lin and S.-J. Chuang, "A filtering microstrip antenna array," *IEEE Trans. Microw. Theory Techn.*, vol. 59, no. 11, pp. 2856–2863, Nov. 2011.

[2] C. X. Mao, Y. Wang, Z. Wang, F. Qin, B. Sanz-Izquierdo, and Q.-X. Chu, "An integrated filtering antenna array with high selectivity and harmonics suppression," *IEEE Trans. Microw. Theory Tech.*, vol. 64, no. 6, pp. 1798–1805, Jun. 2016.

[3] K.-Z. Hu, M.-C. Tang, M. Li, and R. W. Ziolkowski, "Compact, low-profile, bandwidth-enhanced substrate integrated waveguide filtenna," *IEEE Antennas Wireless Propag. Lett.*, vol. 17, no. 8, pp. 1552–1556, Aug. 2018.

[4] M.-C. Tang, Y. Chen, and R. W. Ziolkowski, "Experimentally validated, planar, wideband, electrically small, monopole filtennas based on capacitively loaded loop resonators," *IEEE Trans. Antennas Propag.*, vol. 64, no. 8, pp. 3353-3360, Aug. 2016.

[5] C.-X. Mao, S. Gao, Y. Wang, F. Qin, and Q.-X. Chu, "Multimode resonator-fed dual-polarized antenna array with enhanced bandwidth and selectivity," *IEEE Trans. Antennas Propag.*, vol. 63, no. 12, pp. 5492–5499, Dec. 2015.

[6] B.-H. Zhang and Q. Xue, "Filtering antenna with high selectivity using multiple coupling paths from source/load to resonators," *IEEE Trans. Antennas Propag.*, vol. 66, no.8, pp. 4320-4325, 2018.

[7] Z.-H. Jiang and D.-H. Werner, "A compact, wideband circularly polarized co-designed filtering antenna and its application for wearable devices with low SAR," *IEEE Trans. Antennas Propag.*, vol. 63, no. 9, pp. 3808–3818, Sep. 2015.

[8] Z.-H. Jiang, M. Gregory, and D.-H. Werner, "Design and experimental investigation of a compact circularly polarized integrated filtering antenna for wearable bio-telemetric devices," *IEEE Trans. Biomed. Circuits Syst.*, vol. 10, no. 2, pp. 328–338, Apr. 2016.

[9] Q.-S. Wu, X. Zhang, and L. Zhu, "Co-design of a wideband circularly polarized filtering patch antenna with three minima in axial ratio response," *IEEE Trans. Antennas Propag.*, vol. 66, no. 10, pp. 5022–5030, Oct. 2018.

[10] Y. Lu, Y. Wang, S. Gao, C. Hua, and T. Liu, "Circularly polarised integrated filtering antenna with polarisation reconfigurability," *IET Microw. Antennas Propag.*, vol. 11, pp. 2247–2252, Dec. 2017.

[11] X.-J. Lin, Z.-M. Xie, P.-S. Zhang, and Y. Zhang, "A broadband filtering duplex patch antenna with high isolation," *IEEE Antennas Wireless Propag. Lett.*, vol. 16, pp. 1937–1940, 2017.

[12] H. Chu, J.-X. Chen, S. Luo, and Y.-X. Guo, "A millimeter-wave filtering monopulse antenna array based on substrate integrated waveguide technology," *IEEE Trans. Antennas Propag.*, vol. 64, no. 1, pp. 316–321, Jan. 2016.

[13] H. Tang, J.-X. Chen, H. Chu, G.-Q. Zhang, Y.-J. Yang, and Z.-H. Bao, "Integration design of filtering antenna with load-insensitive multilayer balun filter," *IEEE Trans. Compon., Packag., Manuf. Technol.*, vol. 6, no. 9, pp. 1408–1416, Sep. 2016.

[14] M.-C. Tang, H. Wang, T.-W. Deng, and R. W. Ziolkowski, "Compact planar Ultrawideband antennas with continuously tunable, independent band-notched filters," *IEEE Trans. Antennas Propag.*, vol. 64, no. 8, pp. 3292–3301, Aug. 2016.

[15] M. Barbuto, F. Trotta, F. Bilotti, and A. Toscano, "Horn antennas with integrated notch filters," *IEEE Trans. Antennas Propag.*, vol. 63, no. 2, pp. 781–785, Feb. 2015.

[16] J. Y. Jin, S. Liao, and Q. Xue, "Design of filtering-radiating patch antennas with tunable radiation nulls for high selectivity," *IEEE Trans. Antennas Propag.*, vol. 66, no. 4, pp. 2125–2130, Apr. 2018.

[17] J. F. Li, Z. N. Chen, D. L. Wu, G. Zhang, and Y. J. Wu, "Dual-beam filtering patch antennas for wireless communication application," *IEEE Trans. Antennas Propag.*, vol. 66, no. 7, pp. 3730–3734, Jul. 2018.

[18] W. Yang, Y. Zhang, W. Che, M. Xun, Q. Xue, G. Shen, and W. Feng, "A simple compact filtering patch antenna based on mode analysis with wide out-of-band suppression," *IEEE Trans. Antennas Propag.*, vol. 67, no. 10, pp. 6244-6253, Oct 2019.

[19] W.-C. Yang, S. Chen, Q. Xue, W.-Q. Che, G.-X. Shen, and W.-J. Feng, "Novel filtering method based on metasurface antenna and its application for wideband high-gain filtering antenna with low profile," *IEEE Trans. Antennas Propag.*, vol. 67, no. 3, pp. 1535–1544, Mar. 2019.

[20] X.-Y Zhang, W. Duan, and Y.-M. Pan, "High-gain filtering patch antenna without extra circuit," *IEEE Trans. Antennas Propag.*, vol. 63, no. 12, pp. 5883-5888, Dec. 2015.

[21] Y. Zhang, X. Y. Zhang, L. H. Ye, and Y. M. Pan, "Dual-band base station array using filtering antenna elements for mutual coupling suppression," *IEEE Trans. Antennas Propag.*, vol. 64, no. 8, pp. 3423–3430, Aug. 2016.

[22] K. Xu, J. Shi, X. Qing, Z. N. Chen, "A Substrate Integrated Cavity Backed Filtering Slot Antenna Stacked With a Patch for Frequency Selectivity Enhancement," *IEEE Antennas Wireless Propag. Lett.,* vol. 17, no. 10, pp. 1910–1914, Oct. 2018.

[23] P.-F. Hu, Y.-M. Pan, X.-Y Zhang, and B.-J. Hu, "A filtering patch antenna with reconfigurable frequency and bandwidth using F-shaped probe," *IEEE Trans. Antennas Propag.*, vol. 67, no. 1, pp. 121–130, Jan. 2019.

[24] W. Duan, X. Y. Zhang, Y.-M. Pan, J. X. Xu, and Q. Xue, "Dual-polarized filtering antenna with high selectivity and low cross polarization," *IEEE Trans. Antennas Propag.,* vol. 64, no. 10, pp. 4188–4196, Oct. 2016.

[25] X.-Y. Zhang, Y. Zhang, Y.-M. Pan, and W. Duan, "Low-profile dual-band filtering patch antenna and its application in LTE MIMO system," *IEEE Trans. Antennas Propag.*, vol. 65, no. 1, pp. 103-113, Jan. 2017.

[26] P. F. Hu, Y. M. Pan, X. Y. Zhang, and S. Y. Zheng, "Broadband filtering dielectric resonator antenna with wide stopband," *IEEE Trans. Antennas Propag.*, vol. 65, no. 4, pp. 2079–2084, Apr. 2017.

[27] Y.-M. Pan, P.-F. Hu, X.-Y. Zhang, and S.-Y. Zheng, "A low-profile high-gain and wideband filtering antenna with metasurface," *IEEE Trans. Antennas Propag.*, vol.64, no.5, pp. 2010-2016, May 2016.

[28] P.-F. Hu, Y.-M. Pan, X.-Y. Zhang, and S.-Y. Zheng, "A compact filtering dielectric resonator antenna with wide bandwidth and high gain," *IEEE Trans. Antennas Propag.*, vol. 64, no. 8, pp. 3645-3651, Aug. 2016.

[29] I. J. Bhal and P. Bhartia, *Microstrip Antenna*. Dedham, MA: Artech House, 1980.

[30] K.-M. Luk, C.-K. Mak, Y.-L. Chow, and K.-F. Lee, "Broadband microstrip patch antenna," *Electron. Lett.*, vol. 34, no. 15, pp. 1442-1443, Jul. 1998.

[31] C. A. Balanis, *Antenna Theory: Analysis and Design*, 3rd edition, New

York: Wiley Interscience, 2005.
[32] J.-S. Hong and M. J. Lancaster, *Microstrip Filters for RF/Microwave Applications*, New York: Wiley, 2001.
[33] D. M. Pozar, *Microwave Engineering*. New York: Wiley, 2005.
[34] C.-X. Mao, S. Gao, and Y. Wang, "Low-profile circularly-polarized filtering antenna with improved bandwidth and gain," in *Proc. 12th European Conference on Antennas and Propagation (EuCAP 2018)*, London, UK, Dec. 2018, pp. 226–229.
[35] P. Jin and R. W. Ziolkowski, "Multi-frequency, linear and circular polarized, metamaterial-inspired, near-field resonant parasitic antennas," *IEEE Trans. Antennas Propag.*, vol. 59, no. 5, pp. 1446–1459, May 2011.

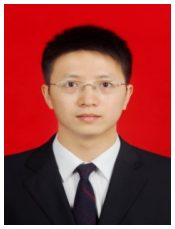

**Ming-Chun Tang** (S'12–M'13–SM'16) received the B. S. degree in physics from the Neijiang Normal University, Neijiang, China, in 2005 and the Ph. D. degree in radio physics from the University of Electronic Science and Technology of China (UESTC), in 2013. From August 2011 to August 2012, he was also with the Department of Electrical and Computer Engineering, The University of Arizona, Tucson, AZ, USA, as a Visiting Scholar. He is currently a full Professor in the School of Microelectronics and Communication Engineering, Chongqing University, China. His research interests include electrically small antennas, RF circuits, metamaterial designs and their applications.

Prof. Tang is the Senior Member of the Chinese Institute of Electronics. He was a recipient of the National Science Fund for Excellent Young Scholars in 2019. He was a recipient of the Best Student Paper Award in the 2010 International Symposium on Signals, Systems and Electronics (ISSSE2010) held in Nanjing, China. His Ph.D. students received Best Student Paper Awards from the IEEE 7th Asia-Pacific Conference on Antennas and Propagation (2018 IEEE APCAP) held in Auckland, New Zealand, 2019 IEEE International Applied Computational Electromagnetics Society (ACES) Symposium held in Nanjing, China, 2019 IEEE International Workshop on Electromagnetics: Applications and Student Innovation Competition held in Qingdao, China, and 2019 Cross Strait Quad-Regional Radio Science and Wireless Technology Conference held in Taiyuan, China. He is the founding Chair of the IEEE AP-S / MTT-S Joint Chongqing Chapter. He serves on the Editorial Boards of several journals, including *IEEE Access*, *Electronics Letters* and *IET Microwaves, Antennas & Propagation*. He has also served on the review boards of various technical journals, and many international conferences as a General Chair, TPC Member, Session Organizer, and the Session Chair.

**Dajiang Li** (S'19) received the B.S. degree from Chongqing Normal University, Chongqing, China, in 2017. He is currently pursuing the Ph.D. degree in School of Microelectronics and Communication Engineering, Chongqing University, Chongqing, China.

His current research interests include filtering antennas and multi-functional antennas and their applications.

**Yang Wang** received the B.S. degree from Southwest University, Chongqing, China, in 2014. He served as a process engineer in SK Hynix Semiconductor (Chongqing) Ltd. from 2014 to 2016. He is currently pursuing the M.S. degree in School of Microelectronics and Communication Engineering, Chongqing University, Chongqing, China.

His current research interests include flexible antennas, and electrically small antennas, quasi-isotropic antennas.

**Kun-Zhi Hu** (S'16) received the B.S. degree and M.S. degree from Chongqing University of Posts and Telecommunications, Chongqing, China, in 2013 and 2016, respectively. He is currently pursuing the Ph.D. degree in circuits and systems with the School of Microelectronics Communication Engineering, Chongqing University, Chongqing, China.

His current research interests include substrate-integrated waveguide components and filtering antennas.

**Richard W. Ziolkowski** (M'87–SM'91–F'94-LF'20) received the Sc. B. (*magna cum laude*) degree (Hons.) in physics from Brown University, Providence, RI, USA, in 1974; the M.S. and Ph.D. degrees in physics from the University of Illinois at Urbana-Champaign, Urbana, IL, USA, in 1975 and 1980, respectively; and an Honorary Doctorate degree, *Doctor Technish Honoris Causa*, from the Technical University of Denmark (DTU), Kongens Lyngby, Denmark in 2012.

Prof. Ziolkowski was the recipient of the 2019 IEEE Electromagnetics Award (IEEE Field Award). He is a Fellow of the Optical Society of America (OSA, 2006) and the American Physical Society (APS, 2016). He served as the President of the IEEE Antennas and Propagation Society in 2005. He is also actively involved with the URSI, OSA and SPIE professional societies. He was the Australian DSTO Fulbright Distinguished Chair in Advanced Science and Technology from 2014-2015. He was a 2014 Thomas-Reuters Highly Cited Researcher.

He is a Distinguished Professor in the Global Big Data Technologies Centre in the Faculty of Engineering and Information Technologies (FEIT) at the University of Technology Sydney, Ultimo NSW, Australia. He became a Professor Emeritus at the University of Arizona in 2018, where he was a Litton Industries John M. Leonis Distinguished Professor in the Department of Electrical and Computer Engineering in the College of Engineering and also a Professor in the College of Optical Sciences. He was the Computational Electronics and Electromagnetics Thrust Area Leader with the Engineering Research Division of the Lawrence Livermore National Laboratory, Livermore, CA, USA, before joining The University of Arizona, Tucson, AZ, USA, in 1990. His current research interests include the application of new mathematical and numerical methods to linear and nonlinear problems dealing with the interaction of electromagnetic and acoustic waves with complex linear and nonlinear media, as well as metamaterials, metamaterial-inspired structures, nano-structures, and other classical and quantum applications-specific configurations.